Templated Platinum/Carbon Oxygen Reduction Fuel Cell Electrocatalysts

ARTICLE *in* THE JOURNAL OF PHYSICAL CHEMISTRY C · FEBRUARY 2010

Impact Factor: 4.77 · DOI: 10.1021/jp909418m

5 AUTHORS, INCLUDING:

Svitlana Pylypenko
Colorado School of Mines
80 PUBLICATIONS **1,338** CITATIONS
SEE PROFILE

Nick J Carroll
Duke University
21 PUBLICATIONS **552** CITATIONS
SEE PROFILE

Dimiter Petsev
University of New Mexico
96 PUBLICATIONS **2,759** CITATIONS
SEE PROFILE

Plamen Atanassov
University of New Mexico
337 PUBLICATIONS **5,293** CITATIONS
SEE PROFILE

Templated Platinum/Carbon Oxygen Reduction Fuel Cell Electrocatalysts

Svitlana Pylypenko,*,† Tim S. Olson,*,† Nick J. Carroll,*,‡ Dimiter N. Petsev,*,‡ and Plamen Atanassov*,†,‡

Center for Emerging Energy Technologies and Center for Biomedical Engineering, Department of Chemical and Nuclear Engineering, University of New Mexico, Albuquerque, New Mexico 87131

Received: September 30, 2009; Revised Manuscript Received: January 21, 2010

This paper describes a new class of templated electrocatalysts for oxygen reduction in polymer electrolyte membrane fuel cells. Electrocatalysts were made by two consecutive procedures. First, porous silica particles were formed by sol−gel synthesis conducted in the aqueous phase of a dispersed system of surfactant micelles and oil microemulsion droplets. This oxide material with bimodal pore size distribution (biporous silica) was then templated by infiltration with solutions of carbon precursor (sucrose) and platinum salt, followed by controlled pyrolysis and dissolution of the silica template. The effect of the bimodal porous structure of the sacrificial silica particles on the structure and oxygen reduction performance of platinum electrocatalysts is discussed. Morphology, composition, and structure of templated carbon support and decorated platinum nanophase were studied through extensive characterization by scanning electron microscopy (SEM) and transmission electron microscopy (TEM), X-ray diffraction (XRD), and X-ray photoelectron spectroscopy (XPS). Optimization of the synthesis conditions resulted in significantly improved performance toward oxygen reduction, evaluated in rotating disk electrode (RDE) and membrane electrode assembly (MEA) configurations.

Introduction

The importance of alternative energy is a well-recognized problem drawing unprecedented attention to research focused toward renewable energy sources. Fuel cell research is yet to grow to be fuel cell technology that is commercially available and affordable. Even though there is no ready solution, directions that fuel cell research should focus on are well understood. First of all, the cost of fuel cells, and therefore electrocatalytic materials have to be reduced. The major research thrust here is advancing currently existing platinum-based materials and lowering loading of precious metals by bringing their utilization to higher levels. Progress was made by alloying platinum with another transition metal,[1–4] and more recently, "de-alloying" of platinum-based alloys.[5,6] Advantages of platinum monolayer[7] and nanostructured thin films[8] approaches were also demonstrated. Materials based on nonprecious metals are another thrust area that can effectively solve cost and supply limitations if their catalytic activity reaches that of precious electrocatalysts.[9] While improving electrocatalysts and electrocatalytic layers and developing new materials is of superior importance, one should always recognize the significance of the issues associated with the durability of fuel cells. Among factors affecting the lifetime of fuel cell operation, dissolution and sintering of platinum particles and corrosion of carbon support are the ones that are most closely related to the properties of electrocatalytic material itself.[10]

A number of limiting parameters, including utilization of the catalyst and corrosion resistance, are strongly affected by the support material. Typically, state of the art electrocatalysts are supported on high surface area carbon blacks. More recently, advances made in the synthesis of high surface area porous carbons[11–13] lead to their further exploration as supports. Applications in catalysis and elecrocatalysis require porous structures where both surface area and transport properties are maximized. Micropores can lead to a better dispersion; however, their accessibly is very limited. Addition of mesopores, on the other hand, can provide an enhancement in the transport by preserving the high surface area necessary to provide efficient dispersion of the precious metal phase. Joo et al. have reported a procedure that utilizes templating of the ordered mesoporous silica with carbon precursors resulting in an ordered carbon that allows high dispersions of platinum particles to be achieved.[14] Following this report a number of publications have centered around the optimization of synthesis of ordered nanoporous carbon.[11–13,15–20] Though high-dispersions of platinum nanophase were shown, performance of electrocatalysts supported on this class of carbon was limited.

Previously, we have exemplified a number of materials obtained through templating with fumed silica and colloidal silica particles. These include nonplatinum electrocatalysts, derived from cobalt and iron porphyrins,[21–28] and platinum-alloy-based electrooxidation catalysts.[29] Recently we have reported on the synthesis of silica particles with bimodal pore sizes obtained through simultaneous templating with microemulsion droplets and micelles and demonstrated their use as templates for the synthesis of platinum-based carbon-supported electrocatalysts.[30] Here, we present a systematic study focused on the synthesis and optimization of this new class of electrocatalysts and investigation of oxygen reduction reaction (ORR) activity, including testing in a single MEA fuel cell.

Experimental Methods

Synthesis of the bimodal porous silica particles that are utilized as the catalyst template was described in our earlier report.[30] Tetraethylorthosilicate (TEOS, Purum >98%) was used as silica precursosr. Cetyltrimethylammonium bromide (CTAB) and modified polyetherpolysiloxane/dimethicone copolyol (ABIL EM 90, Degussa) were employed respectively as water and oil

* To whom correspondence should be addressed.
† Center for Emerging Energy Technologies.
‡ Center for Biomedical Engineering.

10.1021/jp909418m
Published on Web 02/10/2010

phase surfactants. The particles of this material, characterized by bimodal pore size distribution (biporous silica), were impregnated with carbon and platinum precursor solutions by using dry impregnation. The first generation (GEN1) of catalyst materials were synthesized as follows. A solution of carbon precursor was prepared by dissolving sucrose (EMD Chemicals Inc.) in 2 M H_2SO_4 and then adding acetone. Platinum precursor, $H_2PtCl_6 \cdot 6H_2O$ (Sigma-Aldrich), was also dissolved in 2 M H_2SO_4 and mixed with acetone. The loading of platinum varied from 10 to 30 wt %, and the calculation was based on the amount of carbon left after sucrose is decomposed. Silica was impregnated with carbon precursor, and after drying in an oven at 70 °C overnight with platinum precursor. In the synthesis of the second generation (GEN2) of electrocatalysts, silica was impregnated with carbon precursor, dried in the oven at 100 °C for 30 min, then heat-treated at 150 °C for 1 h, and finally impregnated with platinum precursor. Materials were then pyrolyzed in N_2 atmosphere for 4 h, with the ramp rate at 3 deg per min at temperatures ranging from 500 to 1000 °C. To remove the silica template, the powder remaining after pyrolysis was soaked in 6 M KOH solution for 4 days, filtered, washed with DI water, and dried in the oven at 70 °C. The catalyst was also prepared in the following order: impregnation with sucrose precursor, pyrolysis, impregnation with platinum precursor, reduction in N_2/10% H_2 atmosphere for 2 h with a ramp rate at 3 deg per min at 200 °C, and finally KOH etch.

Scanning electron microscopy (SEM) was performed on a Hitachi S-800 instrument and transmission electron microscopy (TEM) was conducted on JEOL 2010 and 2010F instruments. The Brunauer−Emmett−Teller (BET) surface area was determined from nitrogen adsorption/desorption measurements performed on a Quantochrome Autosorb-I-MP instrument. Prior to analysis, samples were outgassed overnight at 120 °C. X-ray photoelectron spectroscopy (XPS) analysis was done using Kratos Axis Ultra XPS with a monochromatic Al Kα source operated at 300 W. XPS data were processed with CasaXPS software. The X-ray powder diffraction (XRD) patterns were obtained on a Scintag diffractometer (Cu K radiation).

Electrochemical characterization was carried out on a Pine Instruments AFCBP1 potentiostat in rotating disk electrode (RDE) configuration. Electrocatalyst solutions were prepared with use of a mixture of DI water, isopropanol (IPA), and Nafion solution (5 wt % Nafion, dilution of 1:10). A thin film was formed on the glassy-carbon electrode with an area of 0.169 cm^2 by applying 10−30 μL from 1 mg/mL ink solution. Cyclic voltammograms were obtained in 0.1 M $HClO_4$ at room temperature with use of a Pt counter and Ag/AgCl reference electrodes.

Single MEA testing was done on a Fuel Cell Technologies, Inc. fuel cell test station, using a 5 cm^2 cell with serpentine flow channel. The anode ink was made by mixing and then sonicating the following: 22.5 mg of platinum black (Aldrich), 800 mg of DI water, 50 mg of 5% Nafion solution, and 100 mL of isopropanol. The cathode ink was prepared in the following way. First, Teflon modified carbon black composite (designated here as "XC-35") is dispersed in the 500 mL of DI water and 200 mg of IPA by sonication. Then 10 mg of electrocatalyst (GEN2 10 wt % Pt/TC - platinum supported on templated catalyst), 151.2 mg of 5 wt % of Nafion solution, 500 mg of DI water, and 400 mg of IPA are added to the dispersion of XC-35 and sonicated. XC-35 carbon black contains about 35 wt % of Teflon and was prepared by a procedure in which PTFE30 (DuPont) and Vulcan XC-72 (Cabot) are mixed. Anode ink solution is hand painted onto a Nafion membrane (N1135, Ion Power, Inc.) placed on a vacuum table at 70 °C. About 90% of the cathode ink was applied to the microporous gas-diffusion material (ELAT GDL LT 1400-W, ETEK) microporous layer and about 10% of the cathode ink was applied directly to a Nafion membrane in a similar fashion to the anode ink. The catalyst coated membrane (CCM) was pressed with GDL layers at 689 N/cm^2 at 125 °C for 5 min. The MEA was tested under the following conditions: H_2 and O_2 gases, heated and humidified at 85 °C and pressurized at 30 psi; 80 °C cell temperature.

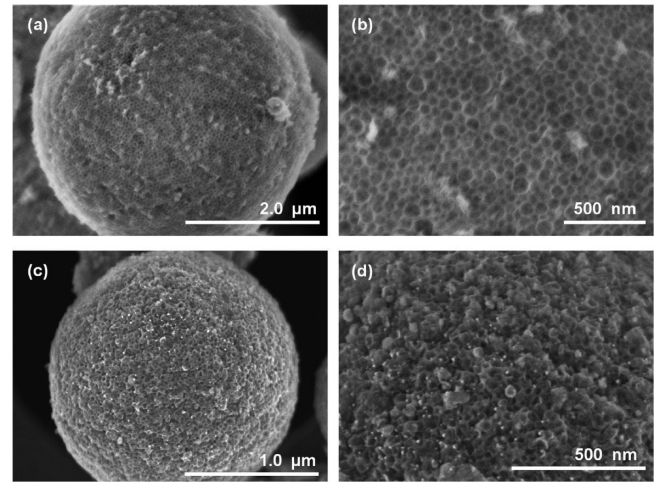

Figure 1. SEM images of (a) silica particle, (b) silica particle at higher magnification demonstrating open structure of the surface, (c) templated carbon particles decorated with platinum nanoparticles, after pyrolysis and silica removal, and (d) templated carbon particles decorated with platinum nanoparticles after pyrolysis and silica removal, at higher magnification demonstrating templated structure.

Results and Discussion

Characterization of Materials. The catalyst materials evaluated in this work were synthesized utilizing the templating of novel silica particles with bimodal porosity (biporous silica). Figure 1 shows SEM micrographs of the silica templating material (Figure 1, parts a and 1b) as well as a Pt/carbon material (Figure 1, parts c and d) after impregnation of the template, pyrolysis, and silica template removal by dissolving it in KOH. TEM micrographs shown in Figure 2 also exemplify silica templating material, and templated carbon and Pt/carbon particles, but here they demonstrate the internal structure and radial distribution of the platinum nanophase. A single silica particle, shown in Figure 1a, represents material obtained by simultaneous templating with micelles and microemulsion droplets.[30] Here, we would like to point out that each silica particle has an internal framework of mesopores (in the range of 10−40 nm) that are connected through a network of nanopores (around 5 nm). Mesopores can be seen in the SEM images in panels a and b of Figure 1 and in the TEM image of the cross-section of the silica particle in Figure 2a. TEM image of the silica cross-section also demonstrates the arrangement of the nanopores. Impregnation of the silica particles with carbon precursor results in the complete filling of silica mesopores. During pyrolysis, the carbon precursor (sucrose) undergoes decomposition and forms a conductive carbon backbone. SEM images in panels c and d of the Figure 1 show templated carbon (TC) particle decorated with platinum nanoparticles after the removal of the silica template. The low (Figures 1a and 1c) and high (Figure 1, parts b and d) magnification images of silica and carbon particles indicate that the structure of the carbon

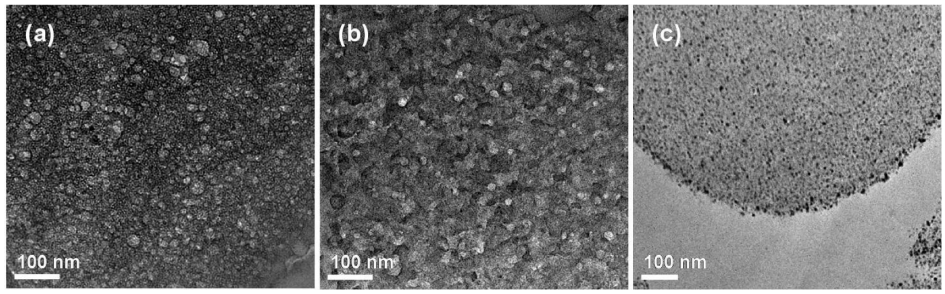

Figure 2. HRTEM micrographs of cross sections of (a) silica particle showing porous structure obtained by templating with micelles and microemulsion droplets, (b) carbon particle after pyrolysis and silica removal demonstrating the internal porous structure, and (c) templated carbon particle decorated with platinum nanoparticles after pyrolysis and silica removal showing the dispersion of platinum nanoparticles.

TABLE 1: XPS Elemental Composition of GEN1 and GEN2 Pt/TC Electrocatalysts

impregnation procedure, sample generation		theoretical Pt loading, wt %	O concn, atom %	C concn, atom %	Pt concn, atom %
C and Pt precursors mixed together	GEN1	30	7.2	92.2	0.6
majority of C precursor (70%), then the rest of C precursor (30%) mixed with Pt precursor	GEN1	30	8.3	90.6	1.1
C precursor, then Pt precursor	GEN1	30	11.2	87.1	1.7
C precursor, then Pt precursor	GEN1	20	11.1	87.9	1.0
C precursor, then Pt precursor	GEN1	10	10.2	89.4	0.4
C precursor, heat-treatment, then Pt precursor	GEN2	10	11.0	88.4	0.7

particles, negative replicas of the biporous silica particles, is dictated by the porous structure of the latter. Further, the internal structure of the carbon is exemplified by TEM analysis of the cross-section of the carbon particle (Figure 2b). The porous structure of the carbon is formed by the voids created after the removal of the silica template. BET surface area measurements for the templated carbon decorated with platinum nanoparticles were found in the range of 400−700 m^2/g depending on the synthesis conditions and loading of platinum.

The distribution of platinum particles supported on the carbon particles was investigated and compared for several GEN1 materials. First, the impregnation procedure was varied. When silica was simultaneously impregnated with platinum and carbon precursors, the amount of surface platinum, as detected by XPS, was quite low (Table 1). Also, a wide distribution of platinum particle size was obtained possibly from locking of platinum nanoparticles not only in the nanopores but also in the mesopores. When the platinum precursor was introduced simultaneously with carbon precursor but after the majority of carbon precursor was already loaded into silica, the amount of surface platinum increased from 0.6 to 1.1 atom % (Table 1) and the average particle size of platinum, observed in TEM (not shown), decreased. Finally, the highest amount of platinum on the surface (about 1.7%) was detected when impregnation with platinum precursor was done after complete impregnation of the carbon precursor (Table 1). Further, the particle size distribution became more monodispersed and the overall dispersion was more homogeneous. Figure 3a is a TEM micrograph of the GEN1 30 wt % Pt/TC material with the highest surface platinum content (platinum precursor impregnation after complete carbon precursor impregnation). The high-magnification image of the same material in Figure 3b illustrates that platinum particles are in the 3−8 nm range and are densely packed. TEM analysis of the cross-section of the particle has shown that platinum nanoparticles are very well dispersed throughout the entire carbon particle (Figure 2c), indicating that the impregnation procedure resulted in the formation of the Pt nanoparticle phase on the surface as well as within the porous network of the templated material.

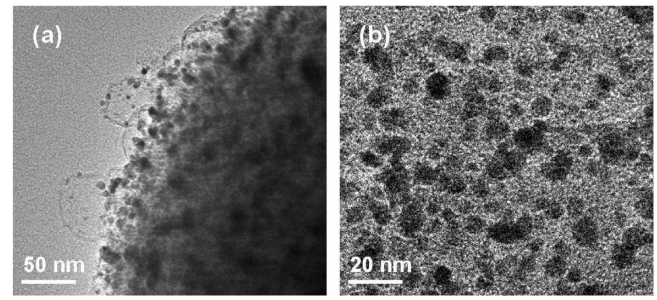

Figure 3. HRTEM images of 30 wt % Pt/TC (a) showing the edge of the carbon particle and (b) higher magnification image demonstrating size and dispersion of platinum nanoparticles.

The effect of the Pt loading on the size and dispersion of the decorating platinum particle phase supported on templated carbon was studied. Table 1 reflects the elemental composition of materials with three different loadings of platinum as determined by XPS. A decrease in the platinum loading results in the nominal decrease in the amount of platinum detected on the surface. For instance, the relative concentration of platinum changes from 1.7% in 30 wt % material to 1.0% and 0.4% in 20 and 10 wt % Pt/TC materials. Reduction in the nominal platinum amount results in less dense dispersion of platinum particles and is accompanied by reduction in their size, as is evident from the TEM analysis of 10 wt % Pt/TC material, shown in Figure 4.

A representative high-resolution Pt 4f spectrum and its deconvolution are shown in Figure 5a. The platinum 4f spectrum consists of two components ($4f_{7/2}$ and $4f_{5/2}$) that are separated by 3.3 eV. Each of the components was curve-fitted with 3 peaks. Peaks at 71.5 eV ($4f_{7/2}$ component) and 74.8 eV ($4f_{5/2}$ component) correspond to metallic Pt. The next double, peaks at 72.3 eV ($4f_{7/2}$ component) and 75.6 eV ($4f_{5/2}$ component), are due to platinum hydroxides, $Pt(OH)_x$. Finally, the last double, peaks at 73.4 eV ($4f_{7/2}$ component) and 76.7 eV ($4f_{5/2}$ component), are contributions of platinum oxides, PtO_x. XPS analysis revealed that the total platinum phase consists of metallic, hydroxide, and oxide forms of approximetaly 35%, 48%, and

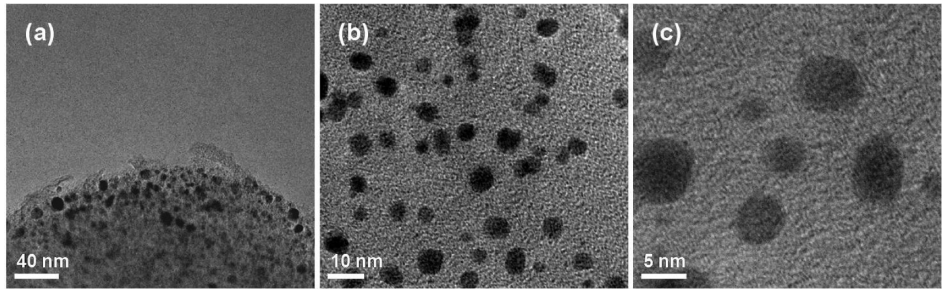

Figure 4. HRTEM images of 30 wt % Pt/TC (a) showing the edge of the carbon particle and (b and c) higher magnification images demonstrating the size and dispersion of platinum nanoparticles.

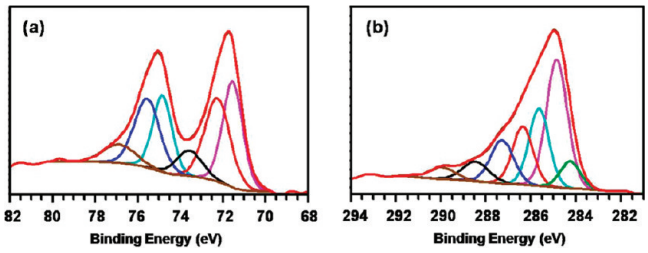

Figure 5. Representative high-resolution XPS spectra of Pt/TC materials: (a) Pt 4f spectrum and (b) C 1s spectrum.

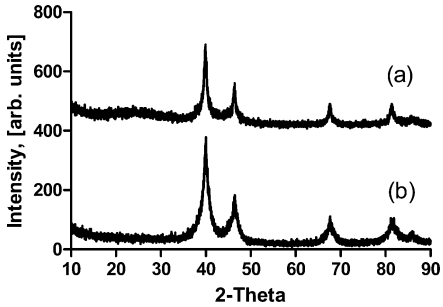

Figure 6. XRD patterns of Pt/TC materials: (a) 10 wt % Pt/TC and (b) 30 wt % Pt/TC.

16% respectively, and is about the same for all Pt/TC materials discussed above. This indicates that only elemental concentrations were affected by the variations in the impregnation steps and platinum loading.

Figure 5b shows a high-resolution C1s spectrum typical of templated carbon decorated with platinum nanoparticles. Several types of carbon species can be distinguished in the C1s spectrum.[31] Amorphous carbon (C—C, at 285 eV) is the major form, while graphitic carbon (C═C, 284.3 eV) is the minor form. Other peaks are due to secondary carbon (C*—C—O, at 285.6 eV) and carbon bonded to oxygen (C—O—C, C—OH, C═O, COOH, located in the range of 286−290 eV). The peak at 291 eV is a shakeup peak, indicative of aromatic/graphitic structure. Only small variations in the carbon speciation were observed for materials with different loading of platinum.

XRD patterns for the 30 wt % and 10 wt % Pt/TC materials shown in panels a and b of Figure 6a are characteristic of carbon-supported platinum electrocatalyst. The shape of the XRD peaks, where the base of the peak is rather wide and the peak around the maximum is rather sharp, indicates that along with small platinum crystallites there is also a fraction of larger crystallite sizes. While smaller crystallite sizes are shown in the TEM images in Figures 2−4, larger crystallite sizes are apparent from the SEM image, shown in panels c and d of Figure 1. Complete quantitative assessment of the Pt nanophase has been hindered at this stage because of the different scale of the data sets (images) observed with SEM and TEM microphotography.

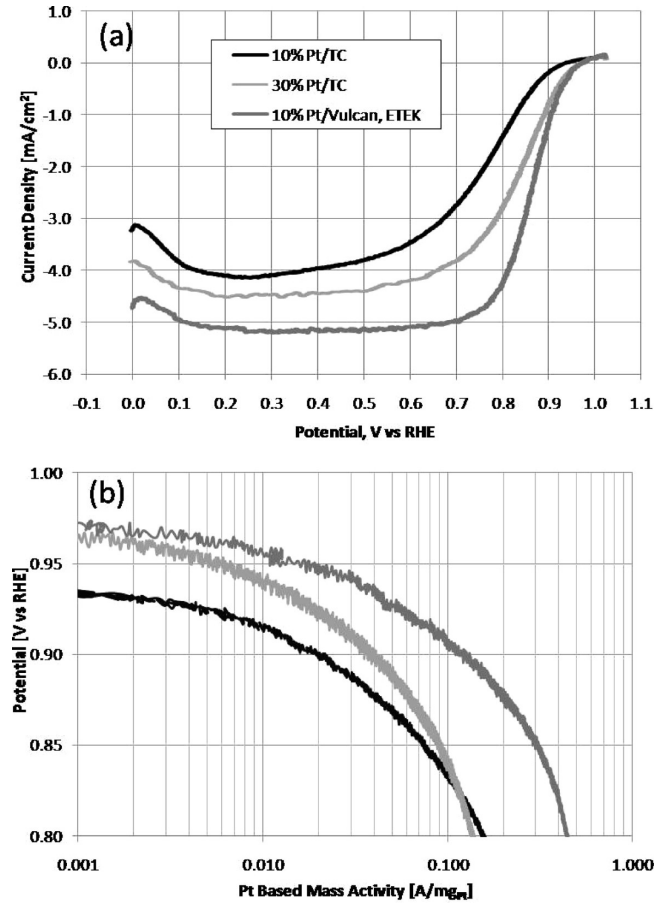

Figure 7. RDE polarization curves in 0.1 M $HClO_4$ solution saturated with O_2 at 25 °C and 1600 rpm. The scan rate is 10 mV/s. The catalyst loading is 9.1 $\mu g_{Pt}/cm^2$ for 10 wt % Pt/TC, 20.5 $\mu g_{Pt}/cm^2$ for 30 wt % Pt/TC, and 9.6 $\mu g_{Pt}/cm^2$ for 10 wt % Pt/Vulcan XC-72R, ETEK.

Electrochemical Characterization of GEN1 Electrocatalysts. Oxygen reduction polarization curves obtained in RDE configuration for 10 and 30 wt % Pt/TC materials are shown in Figure 7a. A 10 wt % Pt on Vulcan XC72 (commercial catalyst) was used as a benchmark. A diffusion-limiting current density of -6 mA cm^{-2}, which is expected for materials that support direct 4 e^- transfer, such as Pt-based electrodes, was not achieved for the template-derived materials or the commercial 10 wt % Pt/C catalyst modified RDE. We are confident in these measurements as others have reported diffusion-limiting current densities ranging between -5 and -6 mA cm^{-2} for RDE-type experiments when utilizing similar commercial catalysts as reported elsewhere.[3,32,33] When compared to commercial, 10 wt

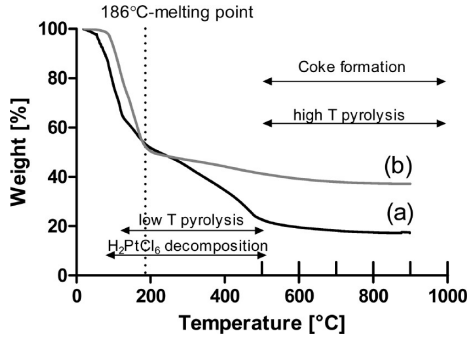

Figure 8. TGA analysis of (a) silica filled with carbon precursor (sucrose) and (b) silica filled with carbon (sucrose) and platinum ($H_2PtCl_6 \cdot 6H_2O$) precursors. Conditions of the TGA analysis simulate conditions of the pyrolysis.

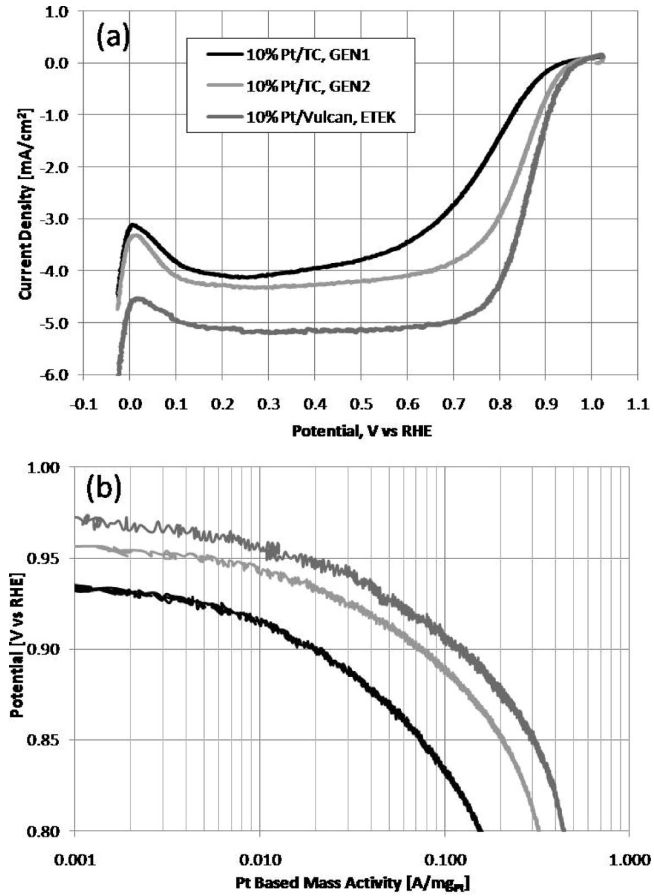

Figure 9. Polarization curves in RDE in 0.1 M $HClO_4$ solution saturated with O_2 at 25 °C and 1600 rpm. The scan rate is 10 mV/s. The catalyst loading is 9.1 $\mu g_{Pt}/cm^2$ for GEN1 and GEN2 10 wt % Pt/TC, pyrolyzed at 900 °C, and 9.6 $\mu g_{Pt}/cm^2$ for 10 wt % Pt/Vulcan XC-72R, ETEK.

% Pt/Vulcan, both templated materials showed significantly lower performance. Lower than expected diffusion-limited currents could be indicative of either a lower number of transferred electrons per redox event and/or additional diffusion limitations in the pores of the templated material. Mass-normalized currents for these materials are shown in Figure 7b. It is clear that intrinsic catalytic activity of GEN1 templated electrocatalysts is lower than that of commercial, Vulcan-supported electrocatalyst. Comparison of templated electrocatalysts with different Pt loading reveals that material with higher Pt loading performs better than material with lower Pt loading. This observation might indicate that limited performance of templated electrocatalysts is caused by contamination, which affects low Pt loading material more than high Pt loading material.

Electrocatalyst Optimization. In search of the reasons of low ORR performance of templated materials, the pyrolysis conditions were simulated in a TGA instrument. The weight losses associated with the changes in the temperature for two unpyrolyzed materials, silica impregnated with sucrose and silica impregnated with sucrose and chloroplatinic acid, are given in Figure 8. Multiple slopes, observed in the TGA graph of sucrose-containing material, indicate that decomposition of the sucrose to a conductive carbon phase is a multiple-step process that is completed when the temperature reaches about 500 °C (Figure 8a). Similar temperature ranges have been reported for sucrose single crystals[34] and in other catalyst synthesis procedures utilizing sucrose as the carbon precursor.[17,20] When the carbon and platinum precursors undergo simultaneous pyrolization (Figure 8b) the weight percent loss is not as large due to the presence of nonvolatile metal atoms. Here, pyrolysis is done in N_2 environment and therefore the only reducing agent present is the carbon precursor material. No further decomposition of sucrose or chloroplatinic acid is observed above 500 °C. It is plausible that coking or Pt-catalyst deactivation may occur in the reported range. Decomposition of the sucrose might result in the coverage of the platinum, decreasing the amount of platinum accessible for participation in the oxygen reduction. Partial decomposition of sucrose at slightly elevated temperatures prior to impregnation with platinum precursor may lead to improved accessibility of platinum. Coking typically occurs at temperatures of 500 °C and higher, and is known to be catalyzed by metals, including platinum. Coking that results in the deactivation of the catalyst active phase cannot be distinguished in the TGA curves shown in Figure 8. To understand if coking is indeed a problem relevant to performance of templated materials the temperature of the pyrolysis can be varied. The optimum synthesis procedure will result in decomposition of both precursors, formation of the conductive carbon phase, and minimization of coking. It appears that 500 °C is the lower end of the temperature range that should be investigated as this is the temperature when decomposition of both precursors is complete.

First, aiming to improve the accessibility of platinum and therefore the precious metal utilization, the impregnation procedure was modified to incorporate an intermediate heat-treatment step. A 10 wt % Pt/TC catalyst sample was made by using heat-treatment performed after impregnation with sucrose precursor but before impregnation with platinum precursor. Only slight improvement in the diffusion-limited region of the ORR polarization curve is achieved with an addition of intermediate heat-treatment (Figure 9a). A diffusion-limiting current density of -6 mA cm^{-2}, which is expected for materials that support direct 4 e^- transfer such as Pt-based electrodes, was not achieved for the template-derived materials or the commercial 10 wt % Pt/C catalyst modified RDE. We are confident in these measurements as others have reported diffusion-limiting current densities ranging between -5 and -6 mA cm^{-2} for RDE-type experiments when utilizing similar commercial catalysts as reported here.[3,32,33] The advancement in the mass-normalized (the theoretical Pt loading was used) currents measured at low overpotentials for this material, shown in Figure 9b, is much more prominent. For instance, ORR activity at 0.9 V increased from 0.02 A/mg_{Pt} to 0.075 A/mg_{Pt}. This result is a major improvement in the performance of the templated electrocatalyst as compared to initial results (GEN1). The initial set of materials,

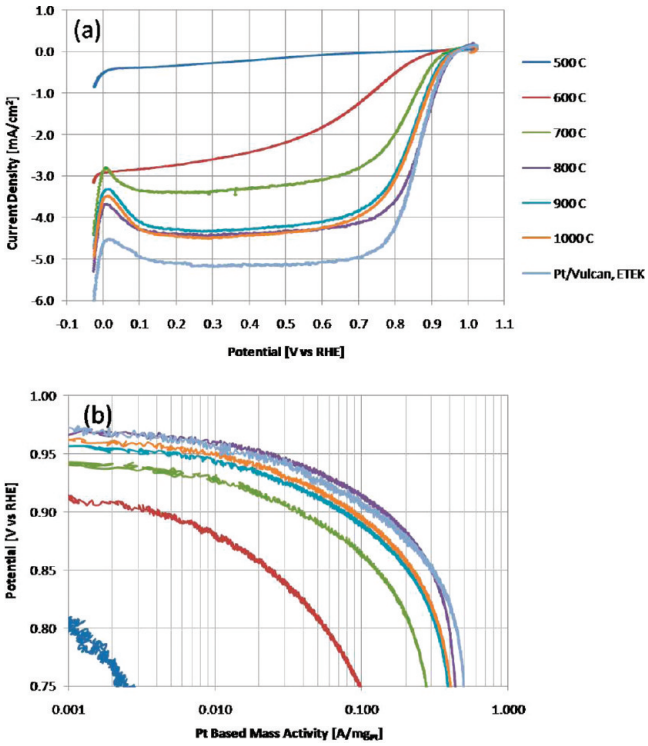

Figure 10. Polarization curves in RDE in 0.1 M $HClO_4$ solution saturated with O_2 at 25 °C and 1600 rpm. The scan rate is 10 mV/s. The catalyst loading is 9.1 $\mu g_{Pt}/cm^2$ for GEN2 10 wt % Pt/TC, pyrolyzed at various temperatures, and 9.6 $\mu g_{Pt}/cm^2$ for 10 wt % Pt/Vulcan XC-72R, ETEK.

made without an intermediate heat-treatment is referred to in the text as the first generation of templated electrocatalysts (GEN1). Materials made by using intermediate heat-treatment are a second generation of templated electrocatalysts (GEN2).

Electrochemical Characterization of GEN2 Electrocatalysts. Next, an intermediate heat-treatment step was utilized during the synthesis of a number of materials. Here, silica material impregnated with sucrose was heat-treated in air at 150 °C for 1 h and then the platinum precursor was added and a second heat-treatment in N_2 was performed at various temperatures. ORR RDE experiment results for materials pyrolyzed at 500, 600, 700, 800, 900, and 1000 °C are shown in Figure 10a. Pyrolysis temperatures lower than 800 °C result in very poor ORR performance, a consequence of poor conductivity of the carbon support. The best ORR performance was obtained when pyrolysis was conducted at 800 °C. Materials for which the temperature of the pyrolysis exceeded 800 °C also exhibited significantly higher ORR performance as compared to materials pyrolyzed at low temperatures. The performance of 800, 900, and 1000 °C treated materials in the diffusion-limited region is quite similar, but lower than expected for Pt-catalyzed ORR under these conditions. It is possible that the Levich equation no longer holds for this system due to the presence of additional diffusion limitations that occur in the mesopores of the Pt/TC-modified RDE. These diffusion limitations are internal with respect to each particle of catalyst. Therefore the number of electrons transferred per redox event cannot be estimated as is often done in the literature. Figure 9b shows the mass-normalized currents that were calculated by using the theoretical platinum loadings. The relative performance of the templated materials becomes more comparable to that of the commercial catalyst. The mass-normalized currents exemplify the utility of the templated catalyst materials measured at low overpotentials.

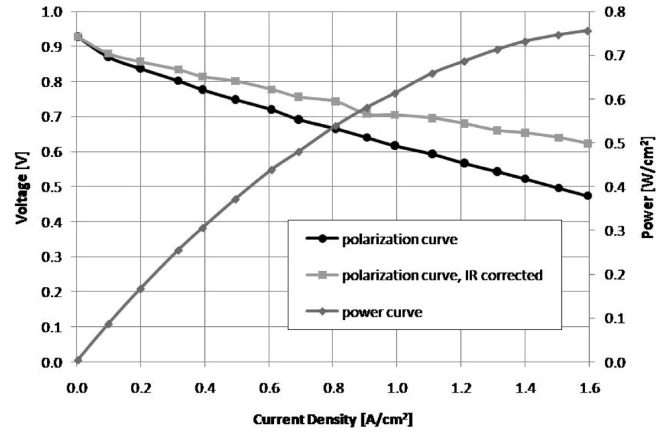

Figure 11. Polarization curves obtained during MEA testing with H_2/O_2 gas feeds heated and humidified at 85 °C and 30 psi backpressure. The cell temperature is 80 °C. The cathode catalyst is GEN2 10 wt % Pt/TC.

However, the mass-normalized currents for the templated materials pyrolyzed at 900 and 1000 °C are observed to be substantially lower than that of the 800 °C treated material. This suggests that the number of electrons transferred during oxygen reduction at temperatures above 800 °C decreases due to an increase in the rate of coke formation during synthesis. The performance of the GEN2 800 °C treated material is very similar, especially in the kinetic region, to that of the commercial Pt/Vulcan catalyst.

The effect of the optimized temperature conditions and addition of the intermediate heat-treatment on the elemental composition of Pt/TC material can be used to explain the improved catalytic activity of the GEN2 electrocatalysts. XPS analysis showed that despite analogous theoretical loading of platinum, surface concentrations of platinum in GEN2 and GEN1 electrocatalysts are different (Table 1). For instance, GEN2 electrocatalyst shows almost twice as much platinum as GEN1 electrocatalyst, and apparently, based on RDE data, the accessibility of the platinum is also much improved.

The material that showed the best RDE performance was also evaluated in MEA configuration with promising results. Single cell fuel cell polarization and power curves obtained for the GEN2 10 wt % Pt/TC electrocatalyst are shown in Figure 11. Aiming at improving hydrophobic−hydrophilic balance and thus transport of oxygen gas to the active sites, XC-35, Teflon-modified Vulcan XC72 carbon black was added to the catalyst ink. Further, to improve the interphase between catalytic and GDL microporous layers, a majority (90%) of the catalyst ink was painted onto the GDL microporous layer and the balance (10%) was directly applied to the Nafion membrane.[21]

Role of Bimodal Porosity of the Template. Typically, when platinum is deposited on the synthetic carbon derived from various carbon precursors, platinum impregnation is done after carbon support is formed (pyrolyzed). This procedure eliminates any problems that could potentially arise when both impregnations are done before the conductive carbon support is formed, including shielding of Pt during the decomposition of the carbon precursor at relatively low temperatures and coking, occurring at higher temperatures. SEM images of the 10 wt % Pt/TC made by impregnation of the pyrolyzed templated carbon are available in Figure 1 in the Supporting Information. The platinum-decorated phase forms large islands made of rather large platinum particles. Apparently, the nanoporous network in silica does not translate into an accessible network in the carbon structure that would effectively lock the size of platinum

particles in the nanosize, as in the case of materials obtained when impregnation with platinum is done before the pyrolysis of carbon.

SEM images of the GEN2 10 wt % Pt/TC, which showed the best RDE performance, demonstrate two types of particles, typical for this material (Figures 2 and 3 in the SI). The first type of particles is formed by complete filling of the mesopores of the template. The rough surface of the carbon particles in this case is due to the voids created after the removal of the template. The second type of carbon particles is formed by incomplete filling of the mesopores in the template. The structure of these carbon particles is formed by the voids, a result of the removal of silica template, and by pores, a result of incomplete filling of the silica mesopores. The two roles of the mesopores in the silica template are to provide channels for effective infiltration with carbon precursor and serve as templates for the carbon mesopores. These, in turn, are expected to serve as channels for the gaseous transport in the catalytic layer during MEA operation. Further optimization of the electrocatalyst will be focused on the optimization of the mesoporous structure of the carbon support.

Both types of carbon particles showed remarkable dispersion of the platinum phase. This emphasizes the essential role of the nanopores in the silica template for the synthesis of the electrocatalysts. Currently, pore size distribution of the nanopores in silica is centered about 5 nm. Their function is to lock platinum particles in the same nanosize range. It is conceivable that decreasing the pore size will lead to the decrease in the platinum particle size, and thus a better utilization of the noble metal. Another potential benefit of the nanoporous network is related to the degradation of electrocatalyst during fuel cell operation. Performance degradation of electrocatalysts is closely related to the growth of platinum particles and their detachment from the carbon support.[10] In the case of platinum supported on templated carbon, these processes might be less pronounced since the mobility of platinum particles is limited as they are locked in the pores.

Conclusions

The current study shows the application of silica particles as templates for fabrication of templated carbon decorated with platinum nanophase for fuel cell catalyst applications. Silica particles have a porous structure with bimodal distribution, created through micelle and microemulsion templating. The bimodal porosity of the silica template is crucial in the synthesis of electrocatalyst as it affects both the structure of the templated carbon and the size and dispersion of the decorated platinum nanophase. Electrocatalysts of GEN1 underperformed as compared to commercial platinum supported on Vulcan carbon black. Issues of contaminations and accessibility of platinum were addressed through optimization of the synthesis procedure by introducing an intermediate heat-treatment of the sucrose/silica material. Oxygen-reduction performance for the GEN2 electrocatalysts showed close to an order of magnitude improvement in ORR activity in RDE measurements. For example, for 10 wt % Pt/TC electrocatalyst ORR activity at 0.9 V, measured in RDE, increased from 0.02 A/mg_{Pt} to 0.15 A/mg_{Pt}. The critical advantage of the novel fuel cell catalyst synthetic method is the degree of control of the decorating platinum nanoparticle phase that can be exercised when templating bimodal porous silica particles. This allows the size platinum nanoparticles to be locked in a desirable size range. Investigation of transport properties and durability studies will be carried out to establish advantages of this class of materials.

Acknowledgment. This work was supported by NSF (PREM/DMR 0611616), NSF (CBET 0828900), DoE-EERE, V.C.7 Advanced Cathode Catalysts (UNM subaward to Los Alamos National Laboratory), and DoE-EPSCoR Implementation Program: Materials for Energy Conversion.

Supporting Information Available: SEM images of 10 wt % Pt/TC obtained by depositing platinum precursor onto material consisting of silica template and pyrolyzed carbon, as well as SEM images demonstrating the two types of structure of GEN2 10 wt % Pt/TC material. This material is available free of charge via the Internet at http://pubs.acs.org.

References and Notes

(1) Mukerjee, S.; Srinivasan, S. *J. Electroanal. Chem.* **1993**, *357*, 201–224.
(2) Mukerjee, S.; Srinivasan, S.; Soriaga, M. P.; Mcbreen, J. *J. Electrochem. Soc.* **1995**, *142*, 1409–1422.
(3) Gasteiger, H. A.; Kocha, S. S.; Sompalli, B.; Wagner, F. T. *Appl. Catal., B* **2005**, *56*, 9–35.
(4) Paulus, U. A.; Wokaun, A.; Scherer, G. G.; Schmidt, T. J.; Stamenkovic, V.; Radmilovic, V.; Markovic, N. M.; Ross, P. N. *J. Phys. Chem. B* **2002**, *106*, 4181–4191.
(5) Koh, S.; Strasser, P. *J. Am. Chem. Soc.* **2007**, *129*, 12624–12625.
(6) Neyerlin, K. C.; Srivastava, R.; Yu, C. F.; Strasser, P. *J. Power Sources* **2009**, *186*, 261–267.
(7) Adzic, R. R.; Zhang, J.; Sasaki, K.; Vukmirovic, M. B.; Shao, M.; Wang, J. X.; Nilekar, A. U.; Mavrikakis, M.; Valerio, J. A.; Uribe, F. *Top. Catal.* **2007**, *46*, 249–262.
(8) Debe, M. K.; Schmoeckel, A. K.; Vernstrorn, G. D.; Atanasoski, R. *J. Power Sources* **2006**, *161*, 1002–1011.
(9) Dodelet, J. P. Oxygen reduction in PEM fuel cell conditions: heat-treated nonprecious metal-N4 macrocycles and beyond. In *N4-macrocyclic metal complexes*; Zagal, J. H., Bedioui, F., Dodelet, J. P., Eds.; Springer Science Business Media Inc.: New York, 2006; pp 83−150.
(10) Borup, R.; Meyers, J.; Pivovar, B.; Kim, Y. S.; Mukundan, R.; Garland, N.; Myers, D.; Wilson, M.; Garzon, F.; Wood, D.; Zelenay, P.; More, K.; Stroh, K.; Zawodzinski, T.; Boncella, J.; McGrath, J. E.; Inaba, M.; Miyatake, K.; Hori, M.; Ota, K.; Ogumi, Z.; Miyata, S.; Nishikata, A.; Siroma, Z.; Uchimoto, Y.; Yasuda, K.; Kimijima, K. I.; Iwashita, N. *Chem. Rev.* **2007**, *107*, 3904–3951.
(11) Lee, J.; Kim, J.; Hyeon, T. *Adv. Mater.* **2006**, *18*, 2073–2094.
(12) Liang, C. D.; Li, Z. J.; Dai, S. *Angew. Chem., Int. Ed.* **2008**, *47*, 3696–3717.
(13) Stein, A.; Wang, Z. Y.; Fierke, M. A. *Adv. Mater.* **2009**, *21*, 265–293.
(14) Joo, S. H.; Choi, S. J.; Oh, I.; Kwak, J.; Liu, Z.; Terasaki, O.; Ryoo, R. *Nature* **2001**, *412*, 169–172.
(15) Raghuveer, V.; Manthiram, A. *Electrochem. Solid-State Lett.* **2004**, *7*, A336–A339.
(16) Chang, H.; Joo, S. H.; Pak, C. *J. Mater. Chem.* **2007**, *17*, 3078–3088.
(17) Kim, T. W.; Park, I. S.; Ryoo, R. *Angew. Chem., Int. Ed.* **2003**, *42*, 4375–4379.
(18) Choi, M.; Ryoo, R. *J. Mater. Chem.* **2007**, *17*, 4204–4209.
(19) Ryoo, R.; Joo, S. H.; Choi, S. J. Ordered mesoporous carbons exhibiting extraordinary metal dispersion. In *Abstracts of Papers*; Proceeding of the 221st ACS National Meeting, San Diego, CA, 2001; American Chemical Society: Washington, DC, 2001; U475.
(20) Joo, S. H.; Jun, S.; Ryoo, R. *Microporous Mesoporous Mater.* **2001**, *44*, 153–158.
(21) Olson, T. S.; Chapman, K.; Atanassov, P. *J. Power Sources* **2008**, *183*, 557–563.
(22) Pylypenko, S.; Mukherjee, S.; Olson, T. S.; Atanassov, P. *Electrochim. Acta* **2008**, *53*, 7875–7883.
(23) Olson, T. S.; Blizanac, B.; Piela, B.; Davey, J. R.; Zelenay, P.; Atanassov, P. *Fuel Cells* **2009**, 9999.
(24) Olson, T. S.; Pylypenko, S.; Fulghum, J. E.; Atanassov, P. *J. Electrochem. Soc.* **2010**, *157*, B54–B63.
(25) Ziegelbauer, J. M.; Olson, T. S.; Pylypenko, S.; Alamgir, F.; Jaye, C.; Atanassov, P.; Mukerjee, S. *J. Phys. Chem. C* **2008**, *112*, 8839–8849.
(26) Artyushkova, K.; Pylypenko, S.; Olson, T. S.; Fulghum, J. E.; Atanassov, P. *Langmuir* **2008**, *24*, 9082–9088.
(27) Artyushkova, K.; Levendosky, S.; Atanassov, P.; Fulghum, J. *Top. Catal.* **2007**, *46*, 263–275.
(28) Jaouen, F.; Herranz, J.; Lefèvre, M.; Dodelet, J.-P.; Kramm, U. I.; Herrmann, I.; Bogdanoff, P.; Maruyama, J.; Nagaoka, T.; Garsuch, A.; Dahn, J. R.; Olson, T.; Pylypenko, S.; Atanassov, P.; Ustinov, E. A. *ACS Appl. Mater. Interfaces* **2009**, *1*, 1623–1639.

(29) Switzer, E. E.; Olson, T. S.; Datye, A. K.; Atanassov, P.; Hibbs, M. R.; Cornelius, C. J. *Electrochim. Acta* **2009**, *54*, 989–995.

(30) Carroll, N. J.; Pylypenko, S.; Atanassov, P. B.; Petsev, D. N. *Langmuir* **2009**, *25*, 1350–13544.

(31) Beamson, G.; Briggs, D. *High resolution XPS of organic polymers: the Scienta ESCA300 database*; Wiley: Chichester: New York, 1992.

(32) Paulus, U. A.; Schmidt, T. J.; Gasteiger, H. A.; Behm, R. J. *J. Electroanal. Chem.* **2001**, *495*, 134–145.

(33) Guilminot, E.; Corcella, A.; Chatenet, M.; Maillard, F. *J. Electroanal. Chem.* **2007**, *599*, 111–120.

(34) Kumaresan, R.; Babu, S. M. *Mater. Chem. Phys.* **1997**, *49*, 83–86.

JP909418M